Journal of Computer Science and Artificial Intelligence
ISSN: 3078-8242 (Print), ISSN: 3078-2309 (Online) | Vol. 9, No. 2, 2026

Phase-Stratified Maximum Independent Set for Periodic Spectrum Capacity Extension

Mengbo Zhai *

College of Energy and Power, Tacheng Vocational and Technical College, Tacheng, 834700, China

* **Corresponding author**: (Email: 1306222022@163.com)

Abstract: Periodic low-duty-cycle reservations can leave recurring gaps that static area-utilization measures do not capture. This study evaluates the capacity for adding C-class devices to a fixed, conflict-free schedule within an unchanged time-frequency box. Each added device is represented by a frequency-band origin and a first-use time; candidates that overlap the baseline are removed, and pairwise conflicts among the remaining placements form a graph. For the C-class period of 10, duration of 2, and bandwidth of 3, candidate conflicts follow an exact modular-phase condition. Five compatible phase classes provide a constructive lower bound, while an exact maximum-independent-set model searches the irregular residual placement graph. Of 52,136 candidate positions, 2,524 survive baseline filtering. The solver certifies 130 added devices, matching its upper bound; a constructive solution contains 90, while area and structural bounds are 675 and 825. Independent checks find no conflict amon g the added plans and the fixed baseline. The results show that periodic phase compatibility and baseline geometry, rather than the count of vacant cells alone, determine usable capacity.

Keywords: Periodic Spectrum Plans, Phase Compatibility, Maximum Independent Set, Capacity Expansion, Conflict-Free Scheduling.

1. Introduction

Recurring wireless transmissions share a finite time-frequency region, but the capacity of that region depends on when each device is active within its cycle, not simply on the sum of nominal bandwidth-duration products. When a device is active for only a small fraction of its period, unused intervals recur in a regular pattern; another device may reuse the same band if its phase is compatible. Recent studies of periodic traffic allocation, sensor scheduling, and adaptive slots show that timing patterns can directly affect collision rates and communication performance [1-4]. Interference-graph models for device-to-device and cellular reuse likewise represent which simultaneous allocations cannot coexist [5-6].

Capacity estimation becomes harder when new periodic plans must fit around a fixed, irregular baseline. A static count of vacant time-frequency cells is insufficient: one candidate position spans a frequency band and many repeated intervals, and it is unusable if any interval intersects an existing plan. Candidate positions may also conflict with one another. For identical periodic profiles, however, relative start times can be reduced modulo the cycle; characterizing forbidden residues exposes phase classes that can coexist. Recent scheduling research uses conflict graphs, independent-set encodings, and multidimensional interference models to select noninterfering transmissions from structured candidate sets [7-10].

This article evaluates additions of C-class devices inside a fixed 100-band by 643-unit time-frequency box. Each added device has the C-class signature and may be placed at any in-range frequency origin and first-use time; movement limits used to repair existing plans do not restrict new placements. Candidate positions are filtered against the frozen conflict-free schedule, then a graph is formed from conflicts among the survivors. A modular compatibility condition simplifies edge generation, while a maximum-independent-set model determines the largest mutually compatible subset. Constructive and resource-area bounds are retained as checks rather than substitutes for exact search.

An exact solver certifies the largest set for this instance, and the resulting placements are independently expanded and checked against the fixed plans and one another. The analysis records the number and geometry of feasible positions, the phase classes used, and the effect of the time horizon and repetition count on capacity. This focus separates capacity extension from schedule repair: the baseline is fixed, and the contribution concerns the placement graph, its periodic compatibility structure, and a certified expansion count. The result distinguishes a weak packing bound from an achievable construction and from the exact maximum.

The resulting count must reflect both cycle structure and the geometry of the positions that remain available.

2. System Model and Fixed Baseline

The capacity calculation holds a conflict-free schedule fixed inside a resource box containing 100 frequency units and a time horizon of 643 units. The candidate additions use the C-class profile: bandwidth 3, occupied duration 2, idle gap 8, and 12 uses. The period is 10, the temporal span is 112, and each plan occupies 72 time-frequency cells. The baseline contains 144 retained plans; no additional frequency bands or time are made available. Its C-class signature and evaluation domain are summarized in Table 1.

Table 1. C-class signature and capacity-evaluation domain.

Quantity	Value	Definition or use
Bandwidth	3	Integer frequency interval width
Occupied duration	2	Time units per use
Idle gap	8	Time units between uses
Repetition count	12	Fixed for every added device
Cycle / temporal span	10 / 112	Duration plus gap; 11 cycle intervals plus one duration
Resource box	100 frequency by 643 time units	Fixed frequency and time limits

A candidate is fully specified by its frequency-band origin and first-use time. The feasible placement domain is:

$$\Pi = \{(\varphi, \theta): 0 \le \varphi \le 97, 0 \le \theta \le 531\}, |\Pi| = 98 \times 532 = 52136 \quad (1)$$

The existing-plan movement limits do not apply to these new placements. Each of the 52,136 candidate positions is tested against all fixed baseline plans; 49,612 are rejected and 2,524 remain available. A candidate is removed if any of its repeated occupied intervals intersects a baseline plan in both frequency and time.

3. Phase Compatibility and the Placement Graph

All new devices have the same period and occupied duration. Two band origins overlap when their separation is at most two units. The complete temporal spans must also intersect; only within that shared span can a modular phase collision occur. The span-overlap test is:

$$T_{mn} = 1 \Leftrightarrow \theta_m < \theta_n + 112 \wedge \theta_n < \theta_m + 112 \quad (2)$$

When the spans overlap, the repeated uses conflict only for phase residues 0, 1, or 9, together with a frequency-band intersection. The resulting pairwise condition is:

$$C_{mn} = 1 \Leftrightarrow (|\varphi_m - \varphi_n| \le 2) \wedge T_{mn} = 1 \wedge ((\theta_m - \theta_n) mod\ 10 \in \{0,1,9\}) \quad (3)$$

The forbidden phase residues are 0, 1, and 9. Selecting phase residues {0, 2, 4, 6, 8} makes distinct selected phases differ by 2, 4, 6, or 8 modulo 10, which avoids the forbidden set. At a shared phase, temporal separation of at least the 112-unit plan span also prevents overlap. Figure 1 illustrates the phase construction and the resulting compatible classes.

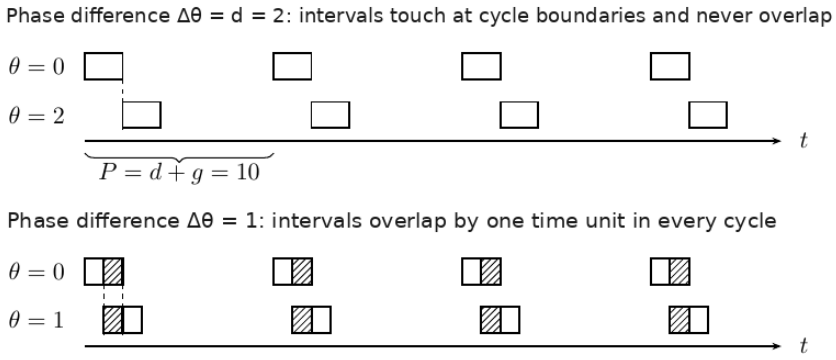

Figure 1. Phase residues that separate repeated occupied intervals.

Each baseline-compatible candidate position becomes a vertex. An edge joins two vertices if their frequency bands and repeated use intervals conflict. A feasible addition set is therefore an independent set of the residual placement graph. A binary decision variable indicates whether each candidate position is selected; the model is:

$$maxN = \Sigma_{m \in V} y_m, y_m + y_n \le 1, \forall (m,n) \in E \quad (4)$$

The preprocessing step removes candidates that are incompatible with the fixed baseline; the graph constraints then prevent conflicts among selected additions. This distinction keeps the search model compact and preserves the exact conflict rule used in the post-solution check.

4. Exact Capacity and Placement Structure

4.1. Bounds and Maximum Independent Set

A structured construction provides a lower bound of 90 additions. Two upper bounds provide checks on the scale of the exact solution. The frequency axis admits at most 33 nonoverlapping width-three bands, the phase construction provides five compatible slots, and at most five nonoverlapping temporal windows fit in the 643-unit horizon, giving a structural bound of 825. An area calculation gives a tighter bound of 675:

$$N \le \lfloor 100/3 \rfloor \times 5 \times \lfloor 643/112 \rfloor = 825, N \le \lfloor (64300 - 15630)/72 \rfloor = 675 \quad (5)$$

The exact maximum-independent-set model is solved with OR-Tools CP-SAT and returns 130 additions with status OPTIMAL and an upper bound of 130; the optimality gap is zero and the reported solve time is 0.29 seconds. Table 2 compares the exact result with the construction and both upper bounds. Figure 2 summarizes the workflow from baseline filtering through exact search.

Table 2. Candidate counts, bounds, and certified capacity.

Measure	Value	Interpretation
Candidate positions	52,136	98 origins and 532 start-time values
Baseline-compatible positions	2,524	After removing 49,612 blocked positions
Constructive lower bound	90	Explicit phase-based feasible placement
Area upper bound	675	Residual cells divided by 72 cells per device
Structural upper bound	825	33 bands × 5 phase classes × 5 windows
Exact maximum	130	Solver upper bound also equals 130

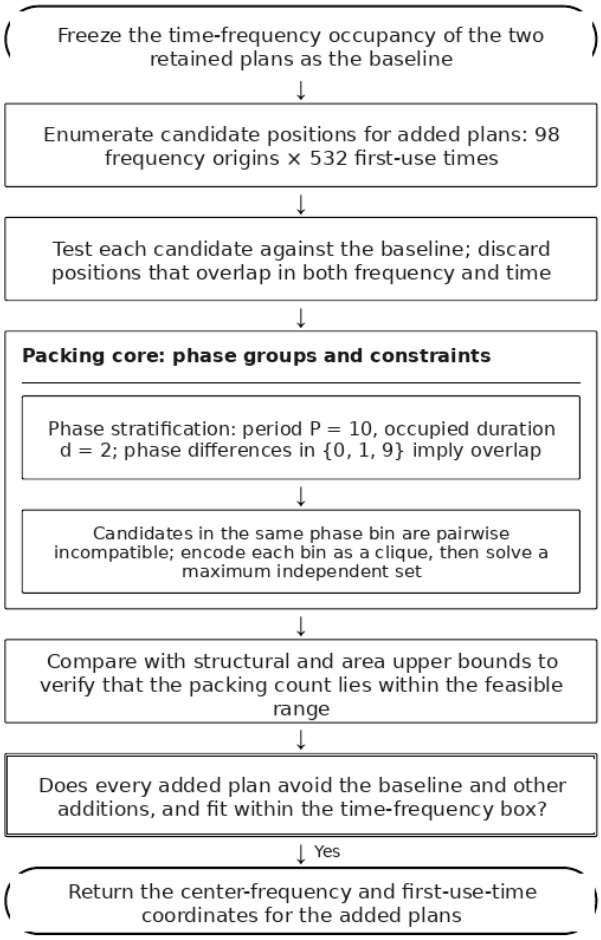

Figure 2. Candidate filtering, phase compatibility, and exact placement search.

4.2. Realized Arrangement and Independent Validation

The 130 placements use 41 distinct frequency strips, and all ten residues modulo 10 appear in the exact solution. The count per phase residue ranges from 8 to 18, while one strip holds at most 16 added devices because different temporal windows can share the same strip. Figure 3 shows both the frozen baseline and the added occupancy in the frequency-time plane, with the accompanying matrix indicating how many added plans use each band origin and phase.

The additions contribute 9,360 occupied cells. The fixed baseline occupies 15,630 distinct cells, so total occupancy rises from 24.31% to 38.86% of the 64,300-cell box. The cell-count increase is consistent with the placements remaining pairwise disjoint; it is not itself a capacity certificate.

For verification, each added plan is regenerated from its frequency origin, first-use time, duration, gap, and repetition count. The independent check tests each added plan against the baseline and against other additions, covering 27,105 relevant plan pairs; no conflict is found and the maximum grid multiplicity is one. Every added position also satisfies the frequency and temporal box limits.

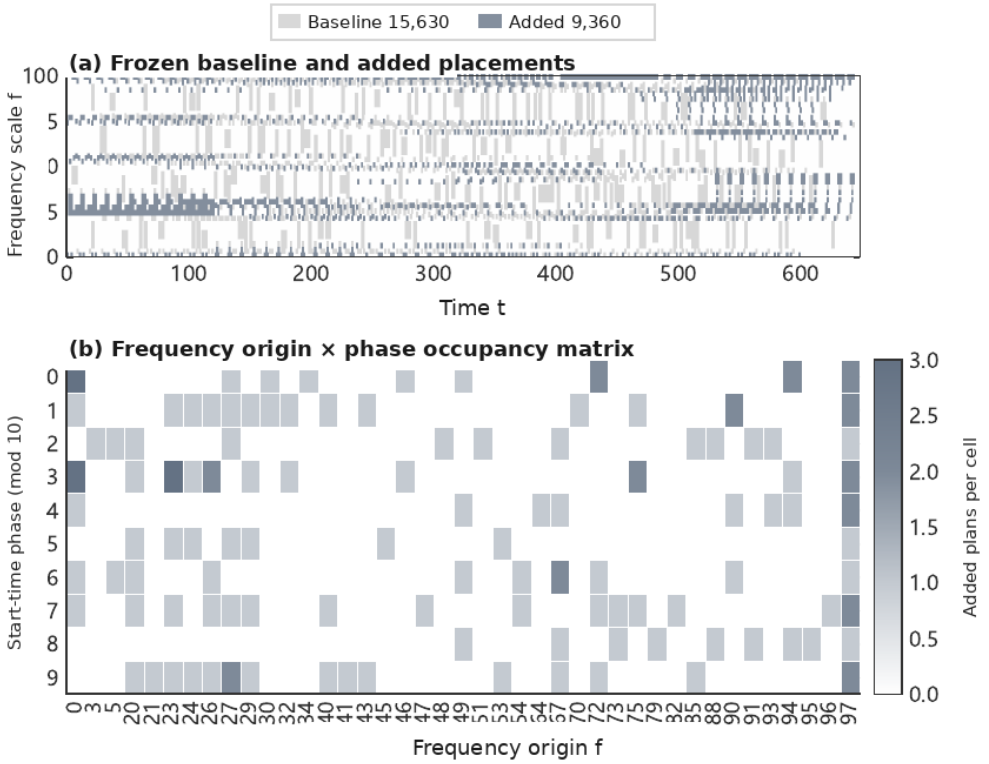

Figure 3. Added placements relative to the fixed baseline and their phase-origin distribution.

5. Parameter Sensitivity and Conclusion

Capacity responds to both the size of the time box and the number of repetitions. Under the same placement procedure, horizons of 600, 643, and 700 units yield 103, 130, and 192 added devices, respectively. Reducing the repetition count from 12 to 6 raises the reported capacity from 130 to 634. These comparisons show that the certified count is specific to the stated C-class profile and resource box; it should not be generalized to a different period or duration without recomputing the compatibility graph. Table 3 summarizes these sensitivity results.

Table 3. Reported capacity under selected sensitivity settings.

Setting	Capacity	Change from baseline case
Horizon 600	103	−27 devices
Horizon 643	130	Reference case
Horizon 700	192	+62 devices
Repetition count 6	634	Compared with 12 uses
Repetition count 12	130	Reference C-class profile

The placement model turns the periodic capacity question into an exact graph problem over complete device placements. Phase residues explain why sparse occupied intervals can coexist on the same band, while the fixed baseline determines which theoretically compatible positions survive in practice. For this case, the solver proves a maximum of 130 additions and independent expansion confirms conflict-free use of the unchanged resource box. The approach therefore combines a periodic compatibility rule, explicit candidate filtering, exact search, and a separately recomputed feasibility check.

References

[1] Kaburaki, A., Adachi, K., Takyu, O., Ohta, M., & Fujii, T. (2023). Resource allocation for periodic traffic in wireless sensor network. In 2023 IEEE Wireless Communications and Networking Conference (WCNC). https://doi.org/10.1109/WCNC55385.2023.10118846

[2] Xie, K., Wu, Z., & Xiong, J. (2023). Optimal periodic sensor scheduling for minimizing communication rate under LQG constraint. Automatica, 156, 111191. https://doi.org/10.1016/j.automatica.2023.111191

[3] Yao, Y., Chen, Y., Yao, H., Ni, Z., & Motani, M. (2023). Multiple task resource allocation considering QoS in energy harvesting systems. IEEE Internet of Things Journal, 10(9), 7893–7908. https://doi.org/10.1109/JIOT.2022.3231869

[4] Yang, Y., Zhang, Y., & Zhuo, Z. (2023). Adaptive time slot resource allocation in SWIPT IoT networks. Computer Modeling in Engineering & Sciences, 136(3), 2787–2813. https://doi.org/10.32604/cmes.2023.027351

[5] Sheu, T. L., Wu, Y. J., & Chiu, Y. C. (2022). Interference-aware and spectral-efficient resource allocation using complete graphs for the D2D communication. Wireless Communications and Mobile Computing, 2022, 3264412. https://doi.org/10.1155/2022/3264412

[6] Sun, C., Huang, G., Shu, J., Yang, Y., & Wu, B. (2024). Joint mode selection and resource allocation based on many-to-many reuse in D2D-aided IoT cellular networks. Internet of Things, 25, 101104. https://doi.org/10.1016/j.iot.2024.101104

[7] Mai, C., Lin, J., & Zhang, W. (2024). Multi-scope spectral graph neural network for link scheduling. In 2024 Boao New Power System International Forum: Power System and New Energy Technology Innovation Forum (pp. 932–940). https://doi.org/10.1109/NPSIF64134.2024.10883477

[8] Zhang, Y., & Guo, D. (2024). Spectrum allocation and scheduling in conflict graphs via scalable multi-agent reinforcement learning. In 2024 58th Asilomar Conference on Signals, Systems, and Computers. https://doi.org/10.1109/IEEECONF60004.2024.10942633

[9] Pu, C., Wei, M., Wang, P, & Hong, S. (2026). Joint deterministic scheduling for multiple coexisting industrial wireless sensor networks via multi-dimensional conflict graphs. Journal of King Saud University Computer and Information

Sciences, 38(6), 552. https://doi.org/10.1007/s44443-026-00982-2

[10] Mallek, A., & Boudhar, M. (2024). Scheduling on uniform machines with a conflict graph: complexity and resolution. International Transactions in Operational Research, 31(2), 863–888. https://doi.org/10.1111/itor.13170